# Chapter 7

## Thallium and Aluminium co-doped ZnO Thin Films

### 7.1 Introduction

Thallium, similar to Al, is a group IIIA element and can substitute the Zn position to give free electrons. $Tl^{+3}$ cations (Tl) being bigger in size as compared to $Al^{+3}$, occupies only substitutional sites [83]. The electron affinity of Tl (~ 0.4 eV) is slightly lower than that of Al (~ 0.43 eV) [322]which makes it more amenable to oxide formation than Al. Thallium oxide acts as an n-type semiconductor due to the vacancy of oxygen, while the defect level of $V_O$ in thallium oxide is just 0.01eV below the conduction band, making it an efficient donor element [323]. Co-doping of thallium with the electronegativity of (1.62), which is slightly lower than that of aluminum (1.61), can result in a cluster formation with a higher possibility of electron donation than AZO [83,85]. This can maximize the charge carrier concentration. At the same time, being a bigger cation $Tl^{+3}$ will have greater s orbital overlap with oxygen 2p orbital resulting in a higher CBM curvature and lower effective mass of the electron, increasing the electron mobility [86,324]. It can be pointed out that the Tl metal is toxic and are not extensively produced [325]. However, $Tl_2O_3$ is very stable and can be utilized in small concentrations as dopants in semiconductor oxides. Therefore, Tl was utilized as a co-dopant along with Al to enhance the conductivity further.

In this chapter, the effect of Tl-doping in ZnO (TZO) and Tl co-doping AZO (TAZO) is experimentally investigated using the solution-processed spray pyrolysis method for the first time. The structural, optical, and electrical properties of TAZO thin film TCO are discussed. The effect of post-deposition radiative annealing in a 5% hydrogen atmosphere on the TZO (TZHO) and Tl-co-doped AZO (TAZHO) has also been investigated.

## 7.2 Results and discussion

### 7.2.1 X-ray diffraction

X-ray diffraction patterns revealed that TZO, TZHO, TAZO, and TAZHO films had hexagonal wurtzite structures (JCPDS#36-1451) [326] as shown in **Figure 7.1**. No oxide impurities of Tl, Al, or related phase were detected from the XRD patterns. TZO and TZHO films had partial orientation along [100] direction [309], while TAZO and TAZHO films were oriented along (002) direction. On radiative annealing, the lattice parameter *'c'* increased, probably due to large atomic radii of Tl and partial hydrogen substitution in place of oxygen-deficient sites during radiative annealing, which causes lattice relaxation [79]. On the other hand, in the case of TAZO the lattice parameter *'c'* did not change significantly on radiative annealing as the ionic radius of Al is smaller than Zn which can balance the expansion due to Tl. In both TZO and TAZO films crystallite size increase on radiative annealing. Crystalline size and d-spacing of TZO, TZHO, TAZO, TAZHO films are mentioned in **Table 7.1**.

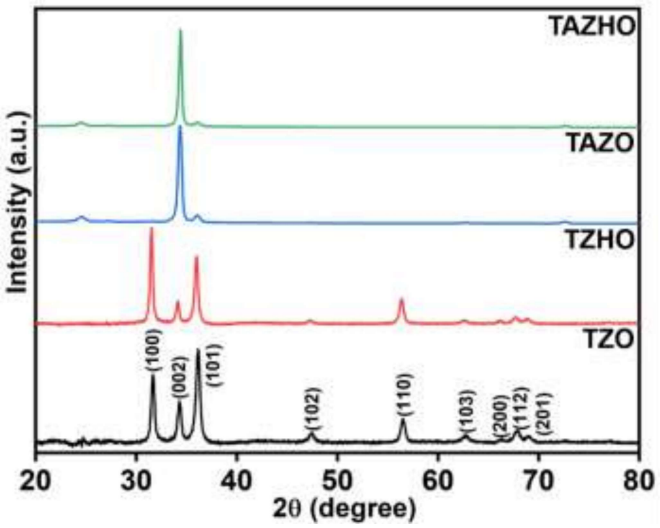


**Figure 7.1** X-ray diffraction pattern of TZO, TZHO, TAZO, and TAZHO films

**Table 7.1** Centre of gravity (COG), FWHM, Crystalline size (nm), d-spacing, and lattice parameter (*c*), of TZO, TZHO, TAZO and TAZHO

| SAMPLE | COG (degree) | FWHM | Crystalline size (nm) | $d_{hkl}$ (Å) | Lattice parameter(*c*), Å |
|---|---|---|---|---|---|
| TZO | 34.30 | 0.44 | 19 | 2.611 | 5.222 |
| TZHO | 34.13 | 0.34 | 24 | 2.624 | 5.248 |
| TAZO | 34.35 | 0.44 | 19 | 2.607 | 5.214 |
| TAZHO | 34.40 | 0.32 | 26 | 2.604 | 5.207 |

## 7.2.2 Scanning Electron Microscopy

SEM images of as-deposited and radiative annealed TZO and TAZO films are shown in **Figure 7.2**. As deposited TZO films were non-uniform and some voids could be observed at the top of the films, as shown in **Figure 7.2a**. On radiative annealing, films became more uniform and homogeneous, as shown in **Figure 7.2b**. TAZO films had uniform grain size, homogeneously distributed all over the substrate surface (**Figure 7.2c)** [83,262]. The grain size (~35 nm) of the TAZO

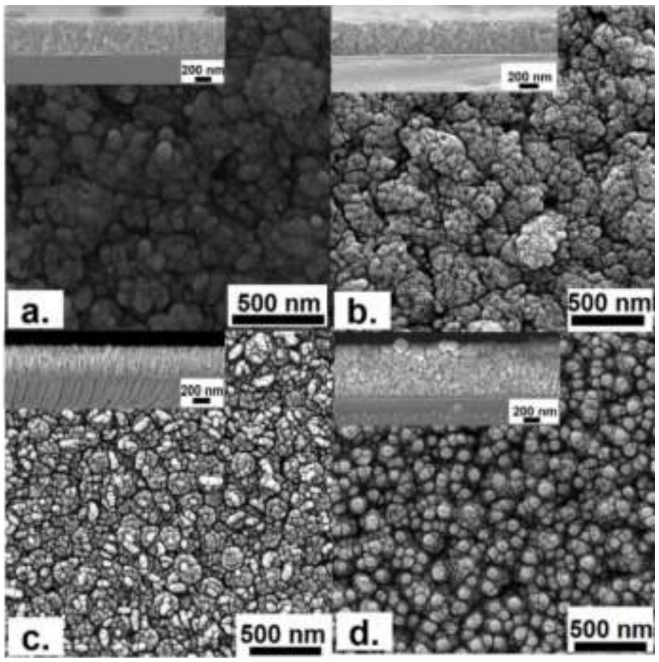


**Figure 7.2** Scanning electron microscopy images of as-deposited and radiative annealed (a) TZO, (b) TZHO, (c) TAZO, and (d) TAZHO films, (inset in each image shows the cross-section).

films was greater than that of TZO and TZHO. On radiative annealing, films (TZHO and TAZHO) became smoother and uniform, as shown in **Figure 7.2b&d**. Cross-sectional images of TZO, TZHO, TAZO and TAZHO films are shown in the respective inset of all the SEM images in **Figure 7.2**. The average thickness of the films was ~550 nm. The inset of **Figure 7.2c** shows that TAZO films had uniform epitaxial grains, while a significant increase in grain size could be observed on radiative annealing (**Figure 7.2d**). The large oriented grains may be one of the reasons for the observed greater mobility in TAZHO films (see subsection **7.2.4**). TZO films had greater resistivity, probably due to the non-uniform morphology and greater voids.

### 7.2.3 Optical properties

To determine the optical properties and the bandgap of the UV–visible spectroscopy was performed. The transmittance of as-deposited TZO and TAZO films in the wavelength range 350-800 nm is shown in **Figure 7.3a**. The transparency of the as-deposited TZO film increased marginally from 75% to 78% after radiative annealing. The transparency of the TAZO film was ~85%, which on radiative annealing in 5% $H_2$ (TAZHO), increased up to ~92% [97,98].

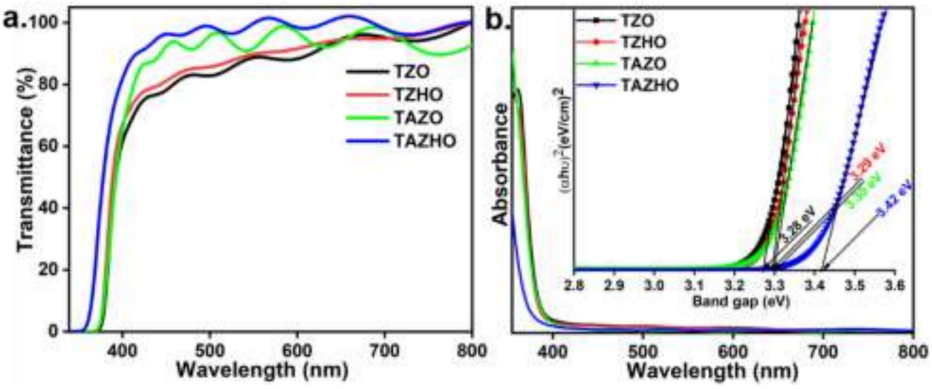


**Figure 7.3** a) Transmittance b) absorbance and Tauc plot in (inset) of TZO and TAZO of as-deposited and radiative annealed thin films

The increase in transparency on radiative annealing could be attributed to the observed improvement in film compactness, increased grain sizes, and reduced scattering centers due to defect passivation (as hydrogen substitutes $V_o$), as observed from XPS spectroscopy. The obtained trend was similar to an earlier report [312]. The optical bandgap energy ($E_g$) was calculated using the Tauc plot, shown in the inset of **Figure 7.3b**. The bandgap of the as-deposited TZO film was ~3.28 ± 0.02 eV on radiative annealing (TZHO), it increased to ~3.29 ± 0.02 eV,

while the as-deposited TAZO film had a bandgap ~3.30 ± 0.02 eV which on radiative annealing (TAZHO) increased to ~3.42 ± 0.02 eV. The bandgap of the Tl-co-doped films was greater in both as-deposited and annealed conditions due to the Burstein Moss shifting [270,327] caused by the increase in charge carrier concentration. In both TZO and TAZO films, the bandgap increased on radiative annealing due to dopant activation and hydrogen passivation of oxygen vacancy.

### 7.2.4 Electrical properties

The electrical properties of the films were characterized using a Hall probe setup. Resistivity was measured at temperatures varying between 295 K to 315 K as shown in **Figure 7.4a**. It has been observed that on radiative annealing (TZHO), the resistivity of the as-deposited TZO film decreased from ~233 Ω-cm to ~$1.54 \times 10^{-1}$ Ω-cm at room temperature. In the case of TAZO films, the resistivity of as-deposited film was ~$2.5 \times 10^{-1}$ Ω-cm, which on radiative annealing in hydrogen (TAZHO films), reduced to ~$9.92 \times 10^{-4}$ Ω-cm at room temperature. Grain growth, hydrogen substitution resulting in passivation of defects, and thallium substitution for Zn are the probable cause of the decrease in the resistivity [83,312]. On increasing the temperature, the resistivity of all the films decreased, except in the case of TAZHO film, when an increase in the resistivity was observed. In the case of TZO, TAZO, and TZHO films, the charge carrier concentration decreased slightly and mobility increased; therefore, the resistivity of the film decreased on heating which is a typical semiconductor behavior. However, in the case of TAZHO film, the charge carrier concentration marginally changed; however, a greater

reduction in mobility was observed which could be attributed to the greater phonon scattering of the charge carrier at a higher temperature, thereby reducing mobility.

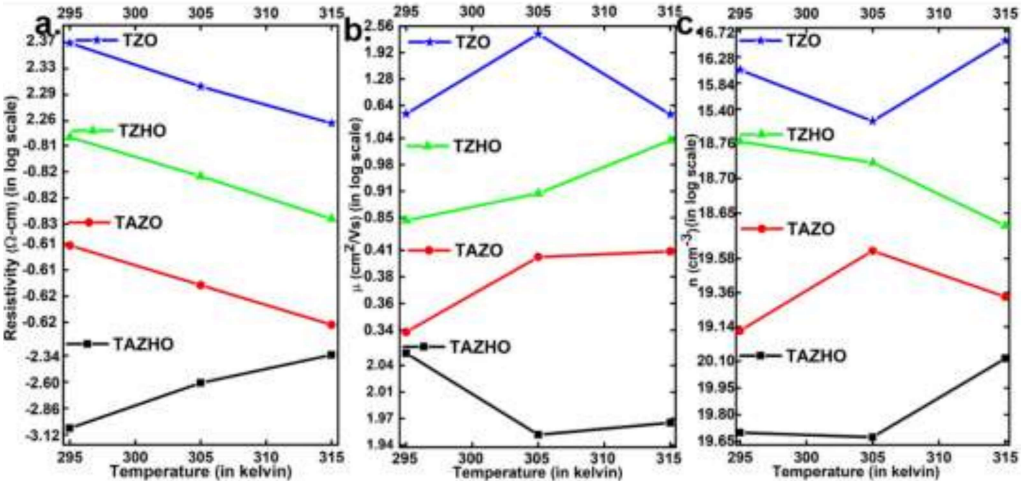


**Figure 7.4** a) Resistivity of the films b) shows the mobility(μ) c) shows the bulk carrier concentration (n) as a function of the temperature of TZO, TZHO, TAZO, and TAZHO films

The mobility and charge carrier concentration was found to improve by an order of magnitude on radiative annealing (**Figure 7.4b&c**). For instance, for TZO film, the mobility and carrier concentration of as-deposited films were ~2.6 $cm^2V^{-1}s^{-1}$ and ~$6x10^{16}$ $cm^{-3}$, which increased to ~$8cm^2V^{-1}s^{-1}$ and ~$5.26x10^{18}$ $cm^{-3}$, respectively, on radiative annealing. The carrier concentration and mobility of as-deposited TAZO films were ~$4x10^{19}$ $cm^{-3}$ and ~3.5 $cm^2V^{-1}s^{-1}$ on radiative annealing charge carrier concentration and mobility of the TAZO films were ~ $2.4x10^{20}$ $cm^{-3}$ and ~56 $cm^2V^{-1}s^{-1}$, respectively. In comparison to the as-deposited TZO films, the carrier concentration of the as-deposited TAZO films was greater while the mobility improved only marginally, which shows the effectiveness of Tl co-doping. This

shows that the Tl being a large element helps in the delocalization of electrons, therefore, improving the charge carrier density, while the radiative annealing in a hydrogen atmosphere tends to passivate the defects, at the same time, can acts as a shallow donor, thereby effectively reducing the resistivity.

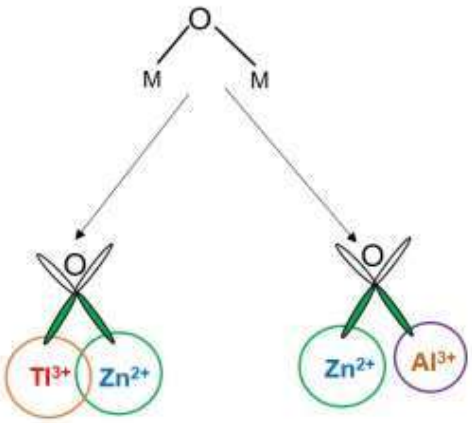


**Figure 7.5** Interaction of s-s orbital for heavy metal cations and light metal cations

$Tl^{3+}$ cation, with electronic configuration $(Xe)4f^{14}d^{10}6s^{0}6p^{0}$, has an outermost shell consisting of s and p orbital. Compared to p orbital, s orbitals are symmetrical overlap with other metal cation $Zn^{2+}$ $(Ar)3d^{10}4s^{0}$ s orbital to form an s-s overlapped cation state as shown in **Figure 7.5**. A wider bandgap and greater overlap of s orbital as compared to $Al^{+3}$ provide greater mobility [328]. Also, the $V_O$ defect state with $Tl^{+3}$ is more stable, resulting in higher bulk carrier concentration in TAZHO films.

### 7.2.5 X-ray photoelectron spectroscopy (XPS)

In order to further investigate the metal-like behavior in the annealed Tl-Al co-doped ZnO films (TAZHO films), XPS of the TAZO (as deposited) and TAZHO

(annealed) films were recorded. XPS peak profiles of the O1s are shown in **Figure 7.6**. O1s peak shape of as-deposited and radiative annealed TAZO film was asymmetric with a tail-like feature towards the higher binding energy. The wide scan of O1s peak of the TAZO and TAZHO films could be deconvoluted into three peaks $O_I$, $O_{II}$, and $O_{III}$, as shown in **Figure 7.6a&b**. The peak at the lower binding energy, close to 530.13 eV (Peak I) in TAZO film, which was attributed to fully co-ordinated oxygen in the lattice ($O_I$) [33,237] shifted to 530.23 eV, while the intensity of the peak increased on radiative annealing (TAZHO film). This showed that the fraction of oxygen bound to (Zn, Al, Tl) regular lattice position increased on radiative annealing in 5% hydrogen atmosphere, which in turn indicated the dopant activation. The second deconvoluted component of O1s peak at a higher binding energy ~530.84 eV [277] (from now on called $O_{II}$) was correlated with $O^{-2}$ ions in the oxygen-deficient region ($O_{Vac}$). Variation in the peak intensity ($O_{II}$) indicated the change in oxygen vacancy concentration. It has been observed from **Figure 7.6b** that ($O_{II}$) peak intensity decreased after radiative annealing, probably due to the dopant activation and defect passivation. The third component of the deconvoluted O1s peak lies at binding energy near to 531.87 eV (from now on $O_{III}$), which can be associated with chemically adsorbed oxygen ($O_{Ads}$) through the atmospheric contaminants such as adsorbed vapors, $-OH^-$ or $-CO_3^{-2}$. After radiative annealing, the intensity of the $O_{III}$ peak decreased significantly. The presence of $O_{Vac}$ (known by the peak $O_{II}$ at ~530.84 eV) plays a significant role in the conductivity of ZnO-based thin films [39,277]. The peak intensity ratio $O_{III}/O_I$ decreased on radiative annealing (TAZHO) as compared to as-deposited film

(TAZO) shown in **Table 7.2.** The reduction in peak intensity ratio $O_{III}/O_I$ was due to the greater electron affinity of aluminum and thallium for oxygen.

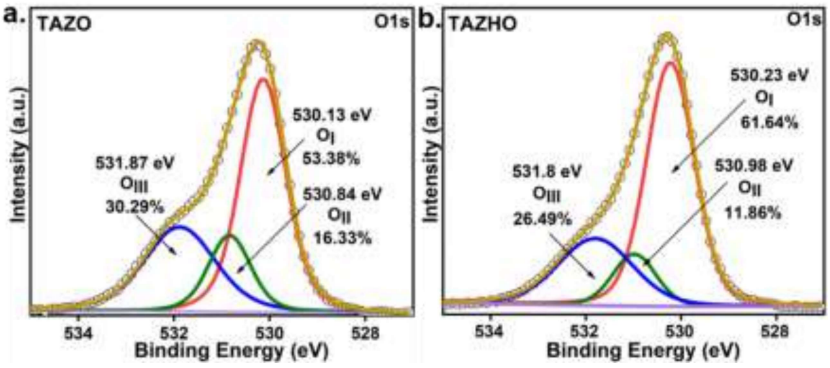


**Figure 7.6** XPS of TAZO a) TAZHO O1s orbital b) XPS of TAZO c) TAZHO Al2p orbital

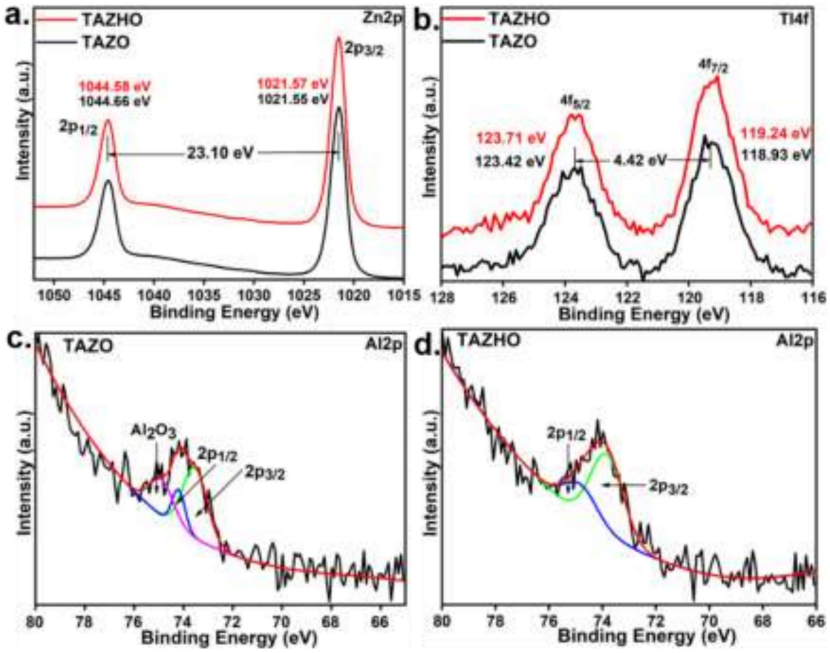


**Figure 7.**7 XPS of Zn 2p orbital a) Tl 4f orbital b) Al 2p TAZO and TAZHO thin film

**Table 7.2** Trend of $O_{Ads}/O_{Lat}$ and $O_{Vac}/O_{Lattice}$ TAZO and TAZHO thin film

| Sample | $O_{Ads}/O_{Lattice}$ | $O_{Vac}/O_{Lattice}$ |
|---|---|---|
| TAZO | 0.57 | 0.31 |
| TAZHO | 0.43 | 0.19 |

It is known that the oxygen-deficient sites are near the conduction band minimum in thallium oxide and act as a shallow donors [323]. After radiative annealing, these oxygen-deficient sites are substituted by hydrogen [312]. Hydrogen substituted at oxygen-deficient sites acts as shallow donors of the electron [54]. Therefore, $O_{Vac}/O_{Lattice}$ ratio reduces slightly after radiative annealing due to the passivating effect of hydrogen. At the same time, the hydrogen incorporation ($H_O$) acts as a shallow donor resulting in enhanced carrier density. XPS spectra of Zn 2p are shown in **Figure 7.7a** of the as-deposited TAZO film Zn $2p_{3/2}$ and Zn $2p_{1/2}$ was located at 1021.55 eV and 1044.58 eV with a spin-orbital split energy gap of 23.1 eV [234]. On radiative annealing, Zn $2p_{3/2}$ and Zn $2p_{1/2}$ peaks shifted to slightly higher binding energies of 1021.57 eV and 1044.66 eV, respectively. This shift of 0.12 eV in Zn 2p peaks was due to the activation of Tl and Al dopants which has a greater affinity for oxygen; as a result, putting the binding electron pairs away from Zn ions in the lattice [324]. XPS of Al 2p orbital in **Figure 7.7c** shows that TAZO has $Al2p_{3/2}$ and $Al2p_{1/2}$ peaks located at 73.54 eV and 74.20 eV, respectively [237]. After radiative annealing (TAZHO) $Al2p_{3/2}$ peak shifted to 73.83 eV, while the intensity of the Al $2p_{3/2}$ peak increased, indicating the dopant activation as shown in **Figure 7.7d** [106,319]. A similar trend was observed in Tl 4f XPS spectra (shown in **Figure 7.7b**). In the case of as-deposited TAZO films, Tl $4f_{7/2}$ and Tl $4f_{5/2}$ peaks

were located at 118.93 eV and 123.42 eV, which on radiative annealing shifted to 119.24 eV and 123.71 eV [324]. The significant increase in the $Tl4f_{7/2}$ orbital binding energies was probably due to the binding of thallium with hydrogen [237].

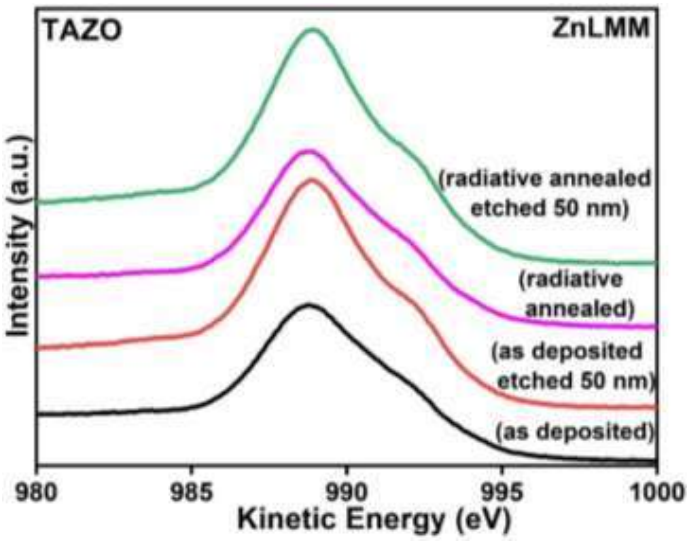


**Figure 7.7** Auger peaks of (ZnLMM) of as-deposited (a) TAZO and, (b) annealed TAZHO films

The chemical state of Zn in TAZO and TAZHO films was examined. The chemical state of the Zn is determined from the energy difference between a representative XPS peak and the most intense auger peak, as shown in **Figure 7.7**. The modified auger parameter ($\beta'$) was calculated using the relation given in Equation 7.1 [287]

$$\beta' = KE(ZnLMM) + BE(Zn2p_{3/2}) \qquad 7.1$$

The modified auger parameter for $Zn2p_{3/2}$ of the TAZO and TAZHO film was 2010.06 eV and 2010.07 eV, respectively, which is close to the modified auger parameter (2010.3 eV) of bulk ZnO. As the top surface of the film is in contact with

the atmosphere, the surface oxidation state will be higher, and lower will be the charge density. A lower value of β indicates a lower electron density around the atom i.e., a higher oxidation state. As the modified auger parameter increases after the etching charge density of the cations increases and the relative oxidation state of the cation decreases, a decrease in oxidation state leads to an increase in electron density [287]. Auger parameter ZnLMM in as-deposited TAZO film increases with the depth of the film from 2010.06 eV to 2010.08 eV shown in Fig.8. In the case of TAZHO film ZnLMM auger parameter (2010.07 eV) increases with the depth (50 nm) to 2010.15 eV.

## 7.3 Concluding Remarks

Heavy cation (Tl) co-doping in AZO, having s-orbital in their outer shell caused greater overlapping of $Tl^{+3}$ and $Zn^{+2}$ leading to increased mobility. At the same, Tl is more electronegative as compared to Al as it forms oxide while Al was easily activated on radiative annealing, thereby increasing the carrier concentration. Dopant activation, the passivating effect of hydrogen substitution, and bigger cation doping lead to increased charge carrier concentration and mobility. Charge carrier concentration and mobility of the TAZHO films were ~$2.4x10^{20}$ $cm^{-3}$ and ~56 $cm^2V^{-1}s^{-1}$, respectively, which gave a minimum resistivity of ~9.92 x $10^{-4}$ Ω-cm. The transparency of the radiative annealed TAZHO film was ~92% in the visible range (350-800 nm).